Chapter 7

Optimized Design of Yb^{3+}/Er^{3+}-Codoped Phosphate Microring Resonator Amplifiers

Juan A. Vallés and R. Gălătuş

Additional information is available at the end of the chapter

http://dx.doi.org/10.5772/61767

Abstract

A precise model to numerically analyse the performance of a highly Yb^{3+}/Er^{3+}-codoped phosphate glass microringresonator (MRR) is presented. This model assumes resonant behaviour inside the ring for both pump and signal powers and considers the coupled evolution of the rare earth (RE) ions population densities and the optical powers that propagate inside the MRR. Energy-transfer inter-atomic processes that become enhanced by required high-dopant concentrations have to be carefully considered in the numerical design. The model is used to calculate the performance of an active add-dropfilter and the more significant parameters are analysed in order to achieve an optimized design. Finally, the model is used to determine the practical requirements for amplification and oscillation in a highly Yb^{3+}/Er^{3+}-codoped phosphate glass MRR side-coupled to two straight waveguides for pump and signal input/output. In particular, the influence of dopant concentration, additional coupling losses and the structure symmetry are fully discussed.

Keywords: Active integrated microring resonators, Yb^{3+}/Er^{3+}-codoped glass, energy-transfer inter-atomic mechanisms, gain/ oscillation requirements, asymmetric structures

1. Introduction

Microring resonators (MRR) have attracted much attention as multifunctional components for signal processing in optical communication systems [1-4]. Recently, due to their fabrication scalability, functionalization and easiness in sensor interrogation, MRR with chip-integrated linear access waveguides have emerged as promising candidates for scalable and multiplexable sensing platforms, providing label-free, highly sensitive and real-time detection capabilities [5-8]. The near-infrared spectral range and, in particular, the 1.5-λm wavelength band is already employed in several bio-/chemical sensing tasks using MRR [9-11].

If gain is incorporated inside the ring, losses (intrinsic absorption, scattering, bend, etc.) can be compensated, filtering and amplifying/oscillating functionalities are combined [12,13] and the sensing potentialities of the device become enhanced [14]. Due to their excellent spectroscopic and solubility characteristics, phosphate glass is a suitable host for rare earth (RE) high doping and Yb^{3+}/Er^{3+}-codoped phosphate glass integrated waveguide amplifiers and lasers provide a compact, efficient and stable performance [15]. However, when the host material of an MRR is Yb^{3+}/Er^{3+}-codoped, the modelling of the performance of the active structure becomes much more complex, since the coupled evolution of the optical powers and the rare earth (RE) ions population densities has to be properly described. Moreover, Er^{3+}-ion efficiency-limiting energy-transfer inter-atomic interactions (homogeneous upconversio n and migration), which are enhanced by high RE-doping levels required by the device dimensions, have to be considered for an optimized design [16].

In the literature, a few models describing RE-doped microfiber ring lasers can be found [17], but there the dopant concentrations level was much lower than those needed in MRRs. Additionally, a simplified model for RE-doped MRR has been proposed where the energy-transfer mechanisms were directly ignored [18]. In a previous paper, we incorporated the effect of high dopant concentrations and presented some results of the optimized active performance of this device [19]. However, in that paper not only the gain coefficient was averaged along the amplifier total length but also the pump resonant behaviour inside the ring and the influence of coupler additional losses were neglected. In subsequent papers we developed a much more detailed model of the performance of a highly Yb^{3+}/Er^{3+}-codoped phosphate glass add-dropfilter filter that overcame previous models deficiencies. An active MRR was described by using a formalism for the intensity rates of the optical powers (pump and signal) at resonance affected by their interaction with the dopant ions through absorption/emission processes. Thus, the performance of an active MRR could be calculated in order to analyse its optimized design and to determine the conditions to achieve amplification and oscillation [20,21].

Drop-port output power maximizing symmetrically coupled structures are mostly used in MRR-based passive components. Alternatively, asymmetric waveguide/MRR coupling may offer definite optimum functional behaviour [22]. For instance, with critically coupled MMRs, the highest throughput attenuation can be attained [23] or when MRR are used as dispersion compensators in the time domain [24].

In this chapter we present a review of our previous works in modelling of Yb^{3+}/Er^{3+}-codoped phosphate microring resonator amplifiers. First, in Section 2, a detailed model of the performance of a highly Yb^{3+}/Er^{3+}-codoped phosphate glass add-drop filter is presented. This model describes the coupled evolution of the rare earth ions population densities and the optical powers that propagate inside the MRR assuming a resonant behaviour inside the ring for both pump and signal powers. In order to exploit the active potentialities of the structure, high dopant concentrations are needed. Therefore, energy-transfer inter-atomic processes are included in the numerical design. The microscopic statistical formalism based on the statistical average of the excitation probability of the Er^{3+} ion in a microscopic level has been used to

http://dx.doi.org/10.5772/61767

describe migration-assisted upconversion. Moreover, due to its high solubility for rare earth ions, phosphate glass is considered an optimum host.

In Section 3, the model is used to calculate the performance of an active microring resonator and the more significant parameters are analysed in order to achieve an optimized design. Finally, in Section 4, the model is used to determine the practical requirements for amplification and oscillation in a highly Yb^{3+}/Er^{3+}-codoped phosphate glass MRR side-coupled to two straight waveguides for pump and signal input/output. In particular, the influence of dopant concentration, additional coupling losses, and the structure symmetry are fully discussed.

2. Yb^{3+}/Er^{3+}-codoped microring resonator model

2.1. Active integrated microring transfer functions

An MRR evanescently coupled to two straight parallel bus waveguides (commonly termed an add-drop filter) is the structure under analysis (see Fig. 1). In our formalism, the add port is ignored since only amplifiers and laser amplifiers are considered. Clockwise direction, single-mode single-polarization propagation is considered. Moreover, the bus waveguides and the MRR are assumed to have the same complex amplitude propagation constant $\beta_c = \beta - j\alpha + jg$. In this expression, β is the phase propagation constant, α is the loss coefficient (due to scattering and bend) and g is the gain coefficient. This coefficient describes the evolution of the pump/signal mode amplitudes caused by their interaction with the RE ions.

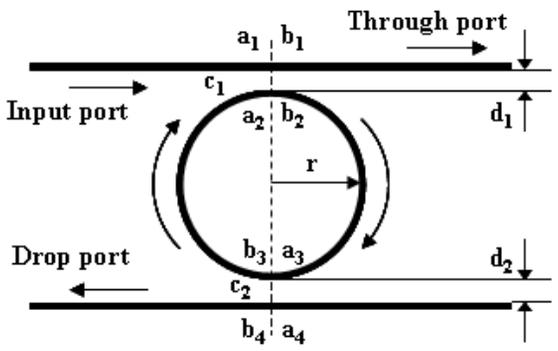

Figure 1. A microring resonator side-coupled to two parallel straight waveguides for pump and signal input/output. The scheme is not to scale.

In Fig. 1 r is the microring radius and the central coupling gaps between each waveguide and the ring are d_i (i=1, 2). Lossless intensity coupling and transmission coefficients at coupler c_i are K_i^0 and T_i^0, satisfying $K_i^0 + T_i^0 = 1$. Correspondingly, $\kappa_i^0 = \left(K_i^0\right)^{1/2}$ and $t_i^0 = \left(T_i^0\right)^{1/2}$ are the lossless amplitude coupling and transmission coefficients. Realistically, we also consider additional coupling losses at the waveguide/microring couplers. Even small additional coupling losses may have a large influence on the MRR performance [20]. Γ_i denotes the coefficient for additional intensity loss at the *ith* coupler. Therefore, the actual intensity

coupling and transmission coefficients are $T_i = (1-\Gamma_i)\,T_i^0$, $K_i = (1-\Gamma_i)\,K_i^0$, which verify the relation $T_i + K_i = (1-\Gamma_i)$, whereas $t_i = T_i^{1/2}$ and $\kappa_i = K_i^{1/2}$ are the amplitude coupling and transmission coefficients, respectively. Mode confinement guarantees that interaction between the microring and bus waveguide cores is negligible outside the coupler regions.

Amplitudes at the couplers output ports. If the input/output complex amplitudes at the couplers ports are denoted as a_i and b_i ($i=1,2$ for the input/through ports at coupler 1 and $i=3,4$ for the add/drop ports at coupler 2, respectively) the following scattering matrix relations can be used to describe the exchange of optical power between the waveguides and the MRR:

$$\text{Coupler I}: \begin{vmatrix} b_1 \\ b_2 \end{vmatrix} = \begin{vmatrix} t_1 & -j\kappa_1 \\ -j\kappa_1 & t_1 \end{vmatrix} \begin{vmatrix} a_1 \\ a_2 \end{vmatrix}; \text{ coupler II:} \begin{vmatrix} b_3 \\ b_4 \end{vmatrix} = \begin{vmatrix} t_2 & -j\kappa_2 \\ -j\kappa_2 & t_2 \end{vmatrix} \begin{vmatrix} a_3 \\ a_4 \end{vmatrix} \tag{1}$$

and the relations between complex amplitudes at the directional couplers ports are:

$$b_1 = t_1 a_1 - j\kappa_1 a_2 \tag{2}$$

$$b_2 = -j\kappa_1 a_1 + t_1 a_2 \tag{3}$$

$$b_3 = t_2 a_3 - j\kappa_2 a_4 \tag{4}$$

$$b_4 = -j\kappa_2 a_3 + t_2 a_3 \tag{5}$$

Moreover, the transmission along the two ring halves is such that

$$a_2 = b_3 \exp(-j\varphi) \tag{6}$$

$$a_3 = b_2 \exp(-j\varphi), \tag{7}$$

where $\varphi = \pi r \beta_c$. Finally, if we assume that the only input signal is in the input port, the amplitudes at the output ports can be straightforwardly derived as:

$$b_1 = \frac{t_1 - (1-\Gamma_1) t_2 \exp(-j2\varphi)}{1 - t_1 t_2 \exp(-j2\varphi)} a_1 \tag{8}$$

$$b_2 = \frac{-j\kappa_1}{1 - t_1 t_2 \exp(-j2\varphi)} a_1 \tag{9}$$

http://dx.doi.org/10.5772/61767

$$b_3 = \frac{-j\kappa_1 t_2 \exp(-j\varphi)}{1 - t_1 t_2 \exp(-j2\varphi)} a_1 \tag{10}$$

$$b_4 = \frac{-\kappa_1 \kappa_2 \exp(-j\varphi)}{1 - t_1 t_2 \exp(-j2\varphi)} a_1 \tag{11}$$

Intensity rates. From Eqs (8)—(11) the input/output transfer functions of the structure in Fig. 1, that is the rates of the intensities from the input port to the coupler output ports, can be readily obtained as follows:

$$I_{11} = \left|\frac{b_1}{a_1}\right|^2 = \frac{t_1^2 + (1-\Gamma_1)^2 t_2^2 \delta^2 - 2(1-\Gamma_1) t_1 t_2 \delta \cos(\beta L)}{1 + t_1^2 t_2^2 \delta^2 - 2 t_1 t_2 \delta \cos(\beta L)} \tag{12}$$

$$I_{21} = \left|\frac{b_2}{a_1}\right|^2 = \frac{\kappa_1^2}{1 + t_1^2 t_2^2 \delta^2 - 2 t_1 t_2 \delta \cos(\beta L)} \tag{13}$$

$$I_{31} = \left|\frac{b_3}{a_1}\right|^2 = \frac{\kappa_1^2 t_2^2 \delta}{1 + t_1^2 t_2^2 \delta^2 - 2 t_1 t_2 \delta \cos(\beta L)} \tag{14}$$

$$I_{41} = \left|\frac{b_4}{a_1}\right|^2 = \frac{\kappa_1^2 \kappa_2^2 \delta}{1 + t_1^2 t_2^2 \delta^2 - 2 t_1 t_2 \delta \cos(\beta L)} \tag{15}$$

where $L = 2\pi r$ is the length of the ring and $\delta = \exp[(g - \alpha)L]$ is the round-trip gain/loss. Mathematically, this structure is analogous to the classical Fabry—Perot interferometer. The output intensities at the through and drop ports correspond to its reflected and transmitted intensities, respectively. If the couplers are lossless, that is $\Gamma_1 = \Gamma_2 = 0$, and there is no ring roundtrip loss, $\delta = 1$, we obtain $I_{11} + I_{41} = 1$. Moreover, if in Eq. (12) $\kappa_2 = \Gamma_2 = 0$, and hence $t_2 = 1$, we obtain the through intensity rate of an all-pass ring resonator with only one coupler:

$$\left|\frac{b_1}{a_1}\right|^2 = \frac{t_1^2 + (1-\Gamma_1)^2 \delta^2 - 2(1-\Gamma_1) t_1 \delta \cos(\beta L)}{1 + t_1^2 \delta^2 - 2 t_1 \delta \cos(\beta L)} \tag{16}$$

Finally, if the intensity rates are considered at the output ends of the straight waveguides, the amplitude evolution from/to the coupler output ports along the add-dropfilter waveguides has to be also taken into account.

2.2. Pump and signal powers evolution inside the active MRR

We assume that the resonance condition ($\beta L = 2m\pi$, where m is an arbitrary integer) is fulfilled for both the pump and signal wavelengths and analyse the evolution of the pump and signal powers inside the MRR.

Then, to determine the intensity rates in Eqs. (12)—(15) not only the passive characteristics of the microring resonator (losses, coupling and transmission coefficients) are required but also pump and signal gain coefficients, which depend on the active MRR working conditions. The evolution of pump and signal powers inside the resonator greatly differ. Whereas signal gain coefficient is habitually be positive even for low pump powers, pump gain coefficient is always negative since pump experiences attenuation along the ring due to absorption by the RE ions.

Pump intensity enhancement inside the ring. The pump power that circulates inside the ring is best described using the intensity enhancement factor, *E*, the rate between the confined and the input intensities, which can be evaluated as the average intensity rate[15]:

$$\begin{aligned} E &= \frac{1}{\pi R}\int_0^{\pi R}\left(I_{21}+I_{31}\right)\exp\left[2\left(g-\alpha\right)\right]dz = \\ &= \frac{1}{\pi R}\int_0^{\pi R}\frac{\kappa_1^2\left\{1+t_2^2\delta\right\}}{\left(1-t_1t_2\delta\right)^2}\exp\left[2\left(g-\alpha\right)\right]dz == \frac{\kappa_1^2\left\{1+t_2^2\delta\right\}}{\left(1-t_1t_2\delta\right)^2}\frac{\left\{1-\delta\right\}}{\left(\alpha-g\right)L} \end{aligned} \tag{17}$$

Signal transfer functions and threshold gain coefficient. For a resonant signal the transfer functions (Eqs. (12) and (15)) become

$$I_{11} = \left\{\frac{t_1-\left(1-\Gamma_1\right)t_2\delta}{1-t_1t_2\delta}\right\}^2,\ I_{41} = \left\{\frac{\kappa_1\kappa_2}{1-t_1t_2\delta}\right\}^2\delta \tag{18}$$

The intensity rate to the through port, I_{11}, cancels when the critical coupling (CC) condition is verified:

$$t_1 = \left(1-\Gamma_1\right)t_2\delta \tag{19}$$

Fulfillment of the CC condition produces the complete destructive interference between the internal field coupled into the output waveguide and the transmitted field in c_1 and, as a consequence, the transmitted intensity drops to zero. From Eq. (18), it can be concluded that if $g-\alpha>0$ (i.e. $\delta>1$),intensity rates I_{11} and I_{41} may be greater than unity and the device is a MRR amplifier. On the other hand if gain compensates all the roundtrip losses and the denominators in Eq. (18) approach zero, I_{11} and I_{41} tend to infinity and the oscillation condition is reached. The threshold gain coefficient, g_{th}, can be calculated as:

http://dx.doi.org/10.5772/61767

$$g_{th} = \alpha_s - \frac{\ln\left[1 - t_1 t_2\right]}{2\pi r} \tag{20}$$

Finally, if $g > g_{th}$, the MRR behaves as a laser amplifier. Therefore, the fulfillment of the oscillation condition depends on the achievable signal gain coefficient, what forces a previous optimizing design based on the active MRR working conditions.

2.3. The Yb^{3+}/Er^{3+}-codoped system in phosphate glass

Due to the large Yb^{3+} absorption cross section in the 980-nm band compared to that of $Er^{3+}$and the good overlapping between the Er^{3+}-ion absorption spectrum ($^4I_{15/2} \Rightarrow {}^4I_{11/2}$) and the Yb^{3+}-ion emission spectrum ($^2F_{5/2} \Rightarrow {}^2F_{7/2}$), ytterbium is a good sensitizer to efficiently improve the gain performance of Er^{3+}-doped waveguide amplifiers. Moreover, because of their high solubility for RE ions and their excellent optical, physical and chemical properties, phosphate glasses stand out among all laser materials for RE-doped waveguide amplifiers and lasers. In particular, high dopant concentrations can be achieved without serious ion clustering [25].

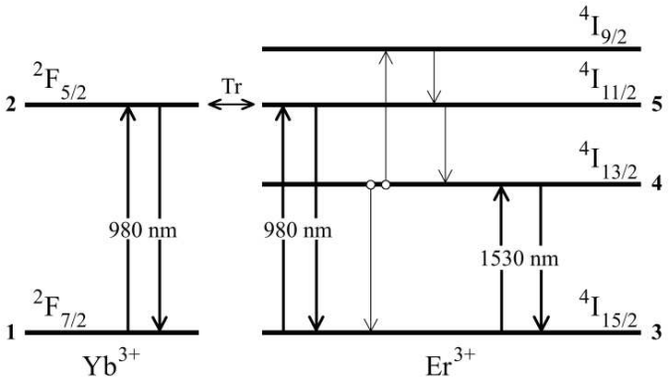

Figure 2. Energy level scheme of the Yb^{3+}-Er^{3+}-codoped system

The schematic energy level diagram of aYb^{3+}/Er^{3+}-codoped phosphate glass system is shown in Fig. 2. We assume the model for a 980-nm pumpedYb^{3+}/Er^{3+}-codoped phosphate glass waveguide amplifier presented in Ref. [16]. In this model the temporal evolution of the population densities of the levels, $n_i (i = 1, 5)$, is described by the rate equations for the Yb^{3+}/Er^{3+}-codoped system, which can be written as follows:

$$\frac{dn_2}{dt} = W_{12} n_1 + C_{BT} n_1 n_5 - [A_2 + W_{21}] n_2 - C_{ET}\left(n_{Yb}\right) n_2 n_3 \tag{21}$$

$$\frac{dn_4}{dt} = W_{34} n_3 - [A_4 + W_{43}] n_4 - 2C_{UP}\left(n_4\right) n_4^2 + A_5 n_5 \tag{22}$$

$$\frac{dn_5}{dt} = -C_{BT} n_1 n_5 + C_{ET}\left(n_{Yb}\right) n_2 n_3 + W_{35} n_3 + C_{UP}\left(n_4\right) n_4^2 - [A_5 + W_{53}] n_5 \tag{23}$$

$$n_1 + n_2 = n_{Yb} \tag{24}$$

$$n_3 + n_4 + n_5 = n_{Er} \tag{25}$$

where the population densities of the ytterbium ion levels $^2F_{7/2}$ and $^2F_{5/2}$, and of the erbium ion levels $^4I_{15/2}$, $^4I_{13/2}$ and $^4I_{11/2}$, are $n_1(x, y, z)$, $n_2(x, y, z)$, $n_3(x, y, z)$, $n_4(x, y, z)$ and $n_5(x, y, z)$, respectively. Notice that, for the sake of simplicity, in Eqs. (21)—(25), the spatial dependence (x, y, z) of the population densities and the densities of stimulated radiative transition rates is omitted. Furthermore, n_{Yb} and n_{Er} denote the homogeneous ytterbium and erbium ions concentrations. In Eqs. (21)—(25), A_i represents the spontaneous relaxation rate from level i, whereas the values of the densities of stimulated radiative transition rates, $W_{ij}(x, y, z)$, can be obtained using the equation

$$W_{ij}(x,y,z) = \sum_{\nu} \frac{\sigma_{ij}(\nu)}{h\nu} \Psi(x,y,\nu) \times P(z,\nu) \tag{26}$$

where $\Psi(x, y, \nu)$ is the normalized mode envelope [26] of the pump, signal or co- and counter-propagating amplified spontaneous emission ($ASE^{\pm}$) waves, with optical frequency ν. $\Psi(x, y, \nu)$ is assumed to be z-independent and depends on the index profile and waveguide profile and the waveguide geometry. Besides, in Eq. (26), $P(z, \nu)$ are the z-propagating total optical powers and $\sigma_{ij}(\nu)$ are the absorption/emission cross sections corresponding to the transition between the *ith* and *jth* levels. Concerning the energy-transfer inter-atomic mechanisms, a term proportional to the Er^{3+}-ion first excited level population squared is used to describe the upconversion effect. The homogeneous upconversion coefficient (HUC) assesses the number of upconversion events per unit time and is a function of the first excited level population, $C_{UP}(n_4)$. Finally, the $Yb^{3+} \Rightarrow Er^{3+}$ energy transfer and back transfer coefficients are $C_{ET}(n_{Yb})$ and C_{BT}, respectively.

We use available parameters from measurements on Yb^{3+}/Er^{3+}-codoped phosphate glass in order to numerically evaluate the Yb^{3+}/Er^{3+}-codoped system rate equations. In particular, the fluorescence lifetime of the Yb^{3+}-ion level $^2F_{5/2}$ is assumed to be 1.1 ms [27], that of the Er^{3+}-ion levels $^4I_{13/2}$and $^4I_{11/2}$are 7.9 ms[28] and 3.6 x 10^5 s^{-1} [29], respectively. Both absorption and emission cross-section distributions for the 1535-nm band are taken from Ref. [30], and the 976-nm pump laser cross sections are taken from Ref. [28] for both ions. According to Ref. [16], for weak CW pump, the HUC coefficient is nearly a constant, whereas for high pump range it is a non-quadratic function of $n_4(x, y, z)$ and saturates at the kinetic limit in the case of infinite pump power [31]. As the Er^{3+} ion concentration increases, the upconversion coefficient also increases due to the migration contribution. This formalism was recently adapted to include

http://dx.doi.org/10.5772/61767

Yb^{3+}-sensitization and transversally resolved rate equations, which become essential due to the nonlinear character of the energy transfer mechanisms.

Concerning the $Yb^{3+} \Rightarrow Er^{3+}$ energy-transfer rate, we assume the fitted values to an experimental dependence of the energy transfer coefficient in [32]. Finally, since the population in the Er^{3+}-ion level $^4I_{11/2}$ remains low even at high pump powers, in practice, the value of the $Er^{3+} \Rightarrow Yb^{3+}$back transfer coefficient can be assumed as a constant, $C_{BT} = 1.5\ x\ 10^{-22} m^3/s$ [33].

Parameter	Symbol	Value
Signal wavelength	λ_s	1534 nm
Pump wavelength	λ_p	976 nm
Decay rate of Yb^{3+2} $F_{5/2}$	A_2	909 s^{-1}
Decay rate of Er^{3+4} $I_{13/2}$	A_4	127 s^{-1}
Decay rate of Er^{3+4} $I_{11/2}$	A_5	3.6 x 10^5 s^{-1}
Absorption cross section $Yb^{3+2}F_{7/2}$ at λ_p	σ_{12}	10.9 x 10^{-25} m^2
Emission cross section $Yb^{3+2}F_{5/2}$ at λ_p	σ_{21}	11.6 x 10^{-25} m^2
Absorption cross section $Er^{3+4}I_{15/2}$ at λ_p	σ_{35}	1.5 x 10^{-25} m^2
Emission cross section $Er^{3+4}I_{11/2}$ at λ_p	σ_{53}	9.6 x 10^{-26} m^2
Absorption cross section $Er^{3+4}I_{15/2}$ at λ_s	σ_{34}	5.4 x 10^{-25} m^2
Emission cross section $Er^{3+4}I_{13/2}$ at λ_s	σ_{43}	5.3 x 10^{-25} m^2
Energy transfer rate $Er^{3+} \Rightarrow Yb^{3+}$ ($^4I_{11/2} + {}^2F_{7/2} \Rightarrow {}^4I_{15/2} + {}^2F_{5/2}$)	C_{BT}	1.5 x 10^{-22} m^3/s
Upconversion critical radius	R_u	9.95 Å
Ratio between critical radii	R_m/R_u	$60^{1/6}$

Table 1. Parameters used for the gain calculations

2.4. Propagation of the optical powers

The evolution along the active waveguide of the pump, signal and ASE powers can be expressed as follows:

$$\frac{dP_p(z,\nu_p)}{dz} = \sigma_{53}(\nu_p)N_5(z,\nu_p) - \sigma_{35}(\nu_p)N_3(z,\nu_p) + \sigma_{21}(\nu_p)N_2(z,\nu_p) - \sigma_{12}(\nu_p)N_1(z,\nu_p) - \alpha(\nu_p) \quad (27)$$

$$\frac{dP_s(z,\nu_s)}{dz} = \sigma_{43}(\nu_s)N_4(z,\nu_s) - \sigma_{34}(\nu_s)N_3(z,\nu_s) - \alpha(\nu_s) \quad (28)$$

In Eqs. (27) and (28), $P_{\gamma}^{\pm}(z, \nu_{\gamma})$ are the optical powers, where z is the distance along the waveguide axis and the label γ is p for pumping and s s for signal. The pump and the signal are assumed to be monochromatic and the wavelength-dependent scattering losses are denoted as $\alpha(\nu_{\gamma})$ and their λ dependence is assumed to follow Rayleigh λ^{-4} law. Finally, in Eqs. (27)—(28) the coupling parameters, $N_i(z, \nu_s)$, are the overlapping integrals between the normalized intensity modal and the *ith* level population density distributions over A, which is the active area,

$$N_i(z,\nu) = \iint_A \Psi(x,y,\nu) n_i(x,y,z) dxdy \tag{29}$$

In Eq. (29), A is defined as the area for which the integral of the addition of population densities of the excited levels converges within a required precision. Finally, a Runge—Kutta-based iterative procedure can be used to numerically integrate the equations that describe the propagation of the optical powers along the waveguide, Eqs. (27) and (28).

3. Numerical analysis of an active add-drop filter

3.1. Passive structure

An air-cladded ridge guiding structure, which presents attractive features for sensing applications [34], has been adopted for the calculations. In Table 2 we summarize the passive parameters of the structure.

Parameter	Value
Waveguide cross section	1.5 μm x 1.5 μm
Substrate refractive index	1.51
Core refractive index	1.65
Pump wavelength	976 nm
Signal wavelength	1534 nm
Pump mode confinement factor	0.962
Signal mode confinement factor	0.757
Microring radius	15.47 μm
Pump wavelength resonant order	156
Signal wavelength resonant order	96
Propagation loss amplitude coefficient	0.25 dB/cm

Table 2. Passive parameters of the structure

The amplitude coupling ratios for pump and signal at each coupler are functions of d_i (i =1, 2). In Fig. 3, we plot the ratios evaluated according to Ref. [35]. Particularly, for the more confined pump power a limited range of values is available.

http://dx.doi.org/10.5772/61767

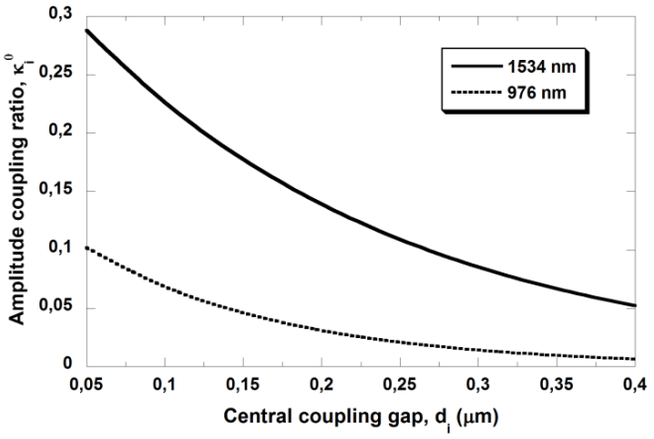

Figure 3. Pump ($\lambda = 976\,nm$) and signal ($\lambda = 1534\,nm$) amplitude coupling ratios as a function of d_i ($i = 1, 2$) [21].

When additional coupling losses are included in the model, the practical range of central coupling gap and accordingly of the amplitude coupling ratio will be further limited. For our analysis the range of additional coupling losses is estimated from Ref. [36], where the value 0.014 is obtained for d=117±5 nm. When the coupling gap between the MRR and the access waveguide is below this value they report a significant increase of these losses.

3.2. Pump enhancement inside the microring

Besides the lossless amplitude coupling coefficient, κ_p^0, and the additional pump coupling loss, Γ_p, the pump intensity enhancement factor, E_p, is basically determined by the pump amplitude gain coefficient, g_p, which reflects the attenuation induced on the pump power by the stimulated transitions in the RE ions. In Fig. 4, E_p is plotted as a function of κ_p^0 for 5 values of g_p with $\Gamma_p = 0.005$. As the pump is more attenuated (the absolute value of g_p increases), the maximum E_p diminishes and is obtained for larger κ_p^0.

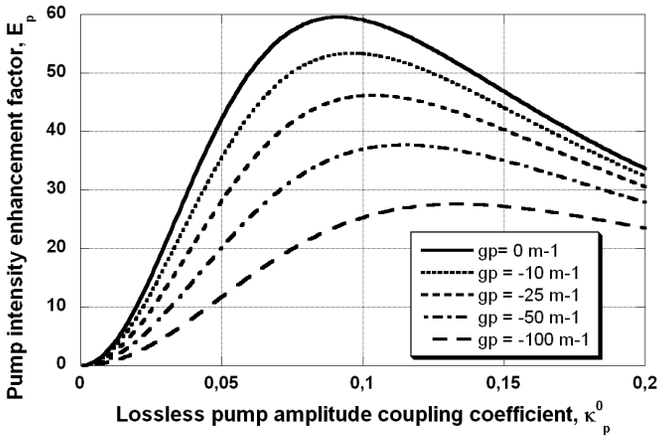

Figure 4. Pump enhancement factor as a function of the lossless amplitude coupling coefficient, κ_p^0, for different values of the pump gain coefficient [20].

Then, using the equations for the coupled evolution of the population densities and optical powers we have calculated the pump amplitude gain coefficient in a waveguide with L = 97.20 μm (2π x 15.47 μm) as a function of the average circulating pump power. This dependence is plotted in Fig. 5 for five concentration pairs (n_{Yb}, n_{Er}) where concentration units are 1 x 10^{26} ions/m^3. RE ions concentration values were chosen with $n_{Yb}= 2n_{Er}$, since this rate is often used experimentally. The amplitude pump gain coefficient varies greatly with the average circulating pump power inside the ring. Low pump powers are strongly attenuated as the dopant concentration increases whereas high pump powers are relatively less affected by rare earth absorption.

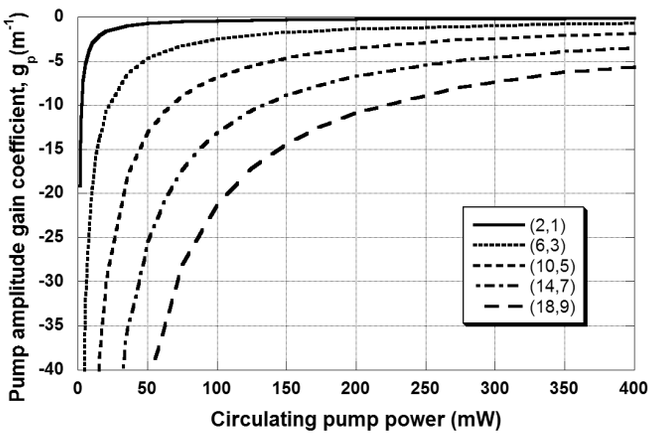

Figure 5. Pump amplitude gain coefficient in a lossless waveguide as a function of the average circulating pump power for five concentration pairs (n_{Yb}, n_{Er}). Units for the RE concentrations are 1 x 10^{26} ions/m^3 [20].

As shown in Fig. 4 and 5, g_p depends on the circulating pump power but, in its turn, E_p is a function of g_p. In practice, for given concentration values, if the required average circulating pump to achieve a signal gain coefficient value is calculated, the associated g_p can be determined, and subsequently, the pump intensity enhancement and the necessary input pump power.

3.3. Signal gain coefficient

First, as with the pump intensity enhancement, we analyse the dependence of the signal intensity rate between the drop and the input ports, I_{41}, on the lossless coupling and on the signal gain coefficient. In Fig. 6, I_{41} is plotted as a function of the signal gain coefficient for four values of the lossless amplitude coupling coefficient and Γ_p=0.005.

For each value of κ_s^0, I_{41} does not grow significantly until g_s approaches the threshold gain (when I_{41} tends to infinity). Then, the input signal is strongly amplified and the rate of growth of I_{41} is higher for lower κ_s^0. Over the gain threshold laser operation is achieved. As we did with g_p, we now calculate g_s as a function of the circulating pump power for five pairs of dopant concentrations.

http://dx.doi.org/10.5772/61767

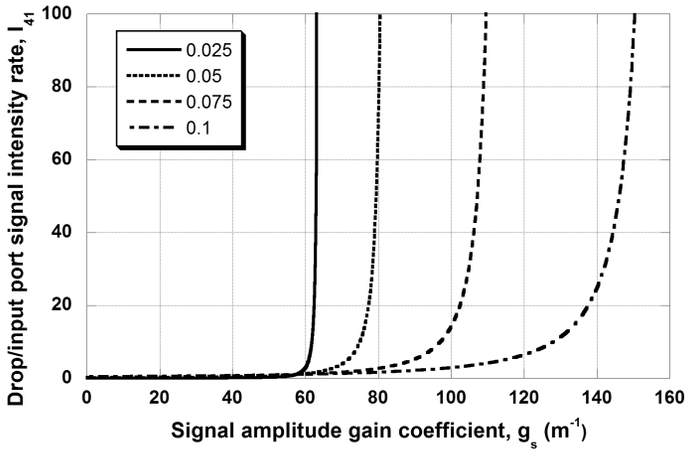

Figure 6. Intensity rate between the drop and the input ports as a function of the signal gain coefficient for four values of the lossless amplitude coupling coefficient κ_s^0 [20].

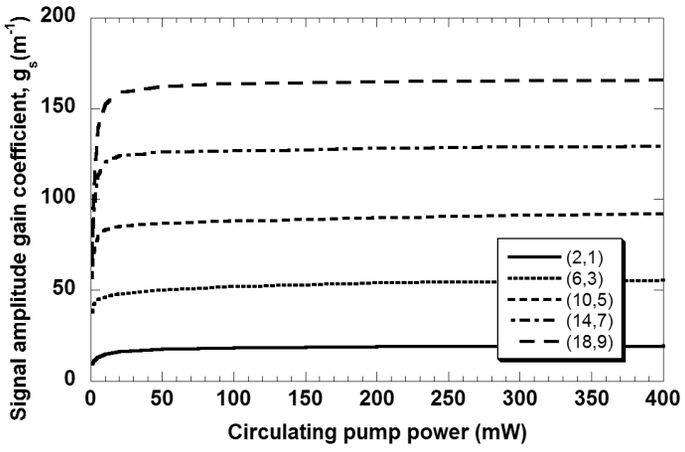

Figure 7. Signal amplitude gain coefficient in a lossless waveguide as a function of the average circulating pump power for 5 concentration pairs (n_{Yb}, n_{Er}). Units for the RE concentrations are 1 x 10^{26} ions/m^3 [20].

As it can be appreciated in Fig. 7, g_s saturates for relatively low circulating pump power for any RE concentration pair. This is caused by the short MRR length, which is much shorter than the waveguide amplifier optimal lengths for each pump power and RE ions concentrations.

By comparing Figs. 6 and 7, the minimum RE ions concentrations necessary to achieve a significant amplification can be estimated as a function of κ_s^0. For instance, if κ_s^0=0.05, amplification becomes significant for $g_s \approx 80\, m^{-1}$. However, to achieve this gain, a high doping level is mandatory, n_{Yb}=$10\, x\, 10^{26}\, ions/m^3$ and n_{Er}=$5\, x\, 10^{26}\, ions/m^3$, approximately. Except for low values (<10 mW), the circulating pump power has a small influence on g_s. For larger values of κ_s^0 the requirement for high doping level is more and more demanding. Therefore, in practice, the available RE doping level limits the value of κ_s^0 for an amplifying MRR and the range of d and the corresponding κ_p^0. For κ_s^0=0.05, the central coupling gap is $d \approx 0.4\, \mu m$ and $\kappa_p^0 \approx 0.006$. According to Ref. [36], for this value of d, low additional coupling losses both for pump and

signal could be feasible. Once κ_p^0 is determined, from Fig. 4 and depending on Γ_p and g_p, the pump intensity enhancement factor, E_p, is obtained and, subsequently, the pump power that has to be the input in the MRR. Although the circulating pump power had a small influence in g_s, together with the RE ions concentrations, determines g_p (see Fig. 5) and E_p.

4. Gain/oscillation requirements for a symmetric structure

4.1. Net gain requirements for a symmetric structure

Firstly, the requirements to achieve net gain and oscillation are going to be analysed in a symmetric structure and afterwards we extend this analysis to asymmetric structures. Therefore, in Sections 4.1 and 4.2, equal lossless amplitude coupling ratios for both pump and signal powers between the microring and the straight waveguides ($\kappa_\lambda^0=\kappa_{1,\lambda}^0=\kappa_{2,\lambda}^0$) and additional coupling losses ($\Gamma_\lambda=\Gamma_{1,\lambda}=\Gamma_{2,\lambda}$) are considered. The net gain that can be obtained in the MRR amplifier is evaluated as:

$$Net\ Gain\ (dB) = 10\log\left(I_{41}\right) \tag{30}$$

Net gain dependence on g_s is plotted in Fig. 8 for three values of κ_s^0 and (a) $\Gamma_s=0.005$ and (b) $\Gamma_s=0.01$.

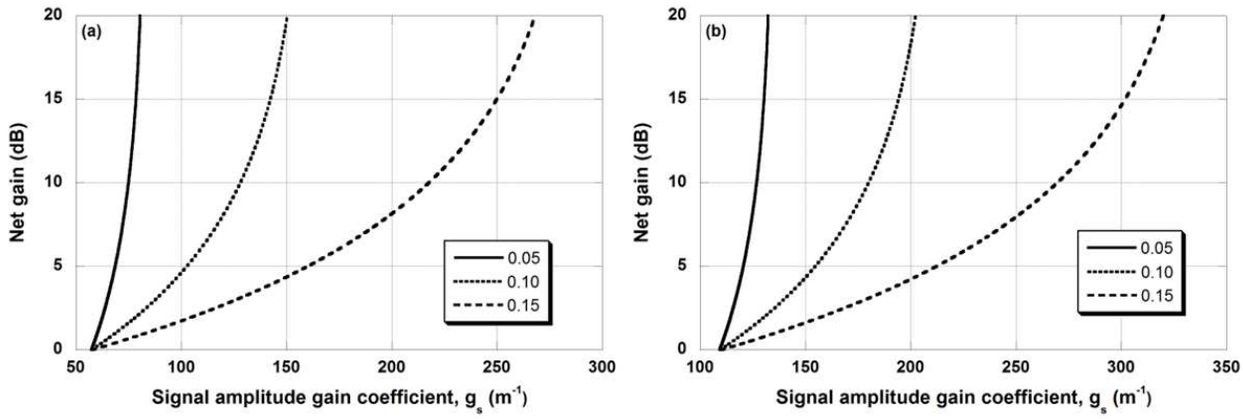

Figure 8. Net gain as a function of g_s for three values of κ_s^0, for (a) $\Gamma_s=0.005$ y (b) $\Gamma_s=0.01$ [21].

As the additional losses increase, the value of g_s (and accordingly of the RE ion concentrations) necessary to achieve positive gain becomes larger. For instance, if $\Gamma_s=0.01$, then $g_s>100\,m^{-1}$, which implies $n_{Er}>7\ x\ 10^{26}m^{-3}$. Once positive net gain is achieved, the rate of growth is higher with lower κ_s^0.

http://dx.doi.org/10.5772/61767

4.2. Threshold gain and oscillation requirements for a symmetric structure

Then, we are going to analyse the oscillation requirements. In Fig. 9, the evolution of the threshold gain as a function of the lossless amplitude coupling coefficient, κ_s^0, for different values of the additional coupling losses is plotted. The great influence on these requirements of Γ_s is clearly appreciated in this figure. As an example, if κ_s^0=0.05, the threshold signal gain coefficient rapidly increases with Γ_s and for Γ_s = 0, 0.005, 0.01 and 0.015, we obtain 31.5 m^{-1}, 83.1 m^{-1}, 134.9 m^{-1} and 187.0 m^{-1}, respectively. Hence, in order to achieve the necessary g_{th}, even small defects in the couplers fabrication process could only be compensated by notably raising the RE doping level. It has to be emphasized that the unavoidable requirements of high RE concentrations impose a host material with a high solubility for RE ions, as phosphate glass where high dopant concentration can be achieved without serious ion clustering [25].

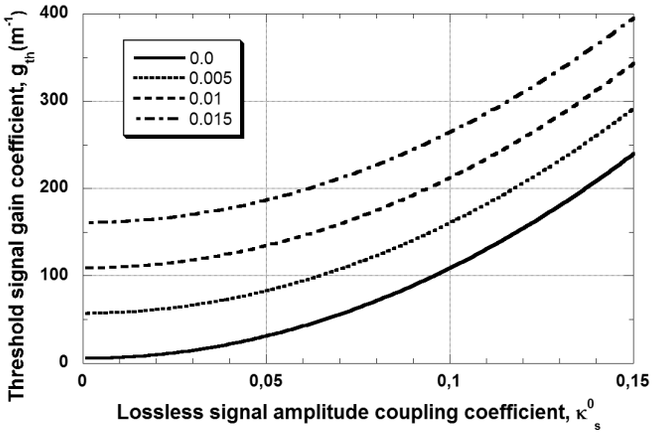

Figure 9. Threshold signal gain coefficient, g_{th}, as a function of the lossless amplitude coupling coefficient, κ_s^0, for four different values of the additional coupling losses Γ_s [21].

A further optimization of the structure could be accomplished if non-symmetric schemes are considered. In the next section we analyse the gain/oscillation requirements when different values for the lossless amplitude coupling ratios and additional coupling losses between each straight waveguide and the microring are allowed.

5. Gain/oscillation requirements for an asymmetric structure

In order to parameterize the asymmetry of the structure, we use the relative variation of the lossless amplitude coupling coefficient, $\Delta\kappa_{r,\lambda}^0$, that is defined as $\Delta\kappa_{r,\lambda}^0 = \left(\kappa_{2,\lambda}^0 - \kappa_{1,\lambda}^0\right) / \kappa_{1,\lambda}^0$. We limit the relative variation between -0.2 and, for simplicity 0.2, we assume the same additional coupling losses for both couplers. A particular attention is going to be paid to active critically-coupled structures and to compare their performance to the passive ones.

5.1. Asymmetry influence on pump enhancement

Pump enhancement presents a maximum as a function of κ_p^0 for each Γ_p in a symmetric structure for a given value of g_p. This maximum shifts towards higher $\kappa_{1,p}^0$ values and rapidly decreases as additional losses increase [20].

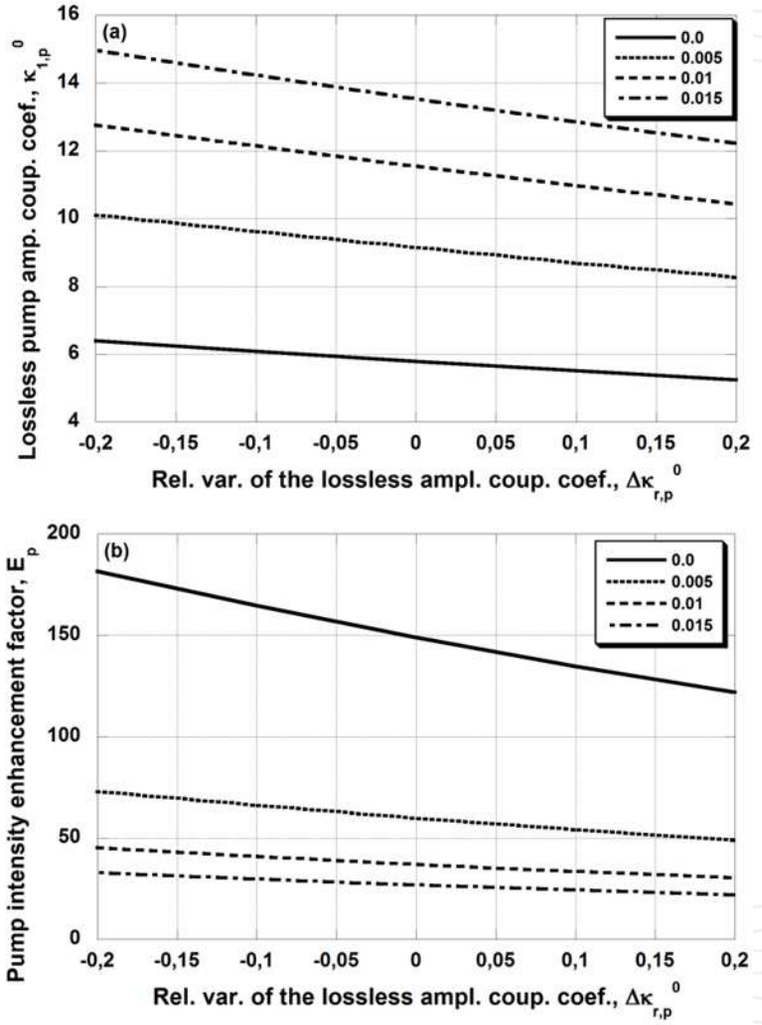

Figure 10. Evolution of the position and value of the pump enhancement maxima as a function of $\Delta\kappa_{r,p}^0$ for different values of $\Gamma_{1,s}$: (a) $\kappa_{1,p}^0$ and (b) E_p [21].

In Fig. 10, the evolution of the maxima position and value are represented as a function of $\Delta\kappa_{r,p}^0$ for different values of $\Gamma_{1,s}$. It is clear from Fig. 6 that $\Delta\kappa_{r,p}^0>0$ (maximum value shifts towards lower κ_p^0) favours pump enhancement (in the limited range of values achievable for κ_p^0 in Fig. 2). The effect of the maximum value reduction is attenuated by the saturation of small signal gain coefficient even for low circulation pump power in Fig. 3(b).

http://dx.doi.org/10.5772/61767

5.2. Asymmetry influence on the drop/input port intensity rate, I_{41}

As we did with symmetric structures, net gain for asymmetric MMR is calculated. In Fig. 11, the evolution with $\Delta\kappa_{r,s}^0$ of the dependence of net gain with g_s for $\kappa_{1,s}^0$=0.1 and $\Gamma_{1,s}$=0.005 is plotted. Although the minimum value of g_s does not change, the rate of growth is larger for $\Delta\kappa_{r,s}^0$<0.

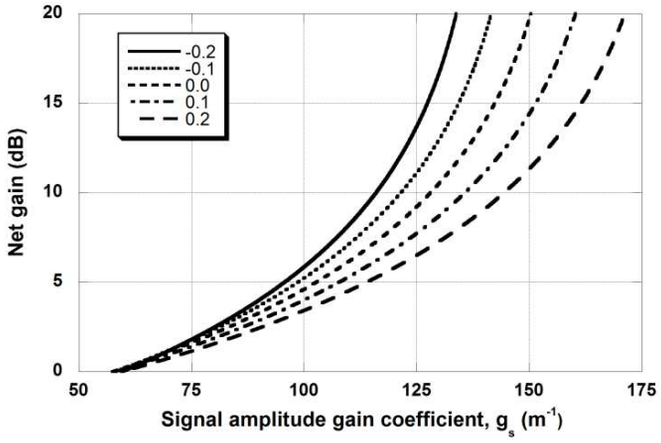

Figure 11. Evolution with $\Delta\kappa_{r,s}^0$ of the dependence of net gain with g_s for $\kappa_{1,s}^0$=0.1 and $\Gamma_{1,s}$=0.005 [21].

Next, we study the performance in CC conditions. Differently from the passive MRR, in an active structure the value of $\kappa_{2,s}^0$ that cancels the throughout intensity depends on the additional losses and on the signal gain amplitude coefficient for a given $\kappa_{1,s}^0$.

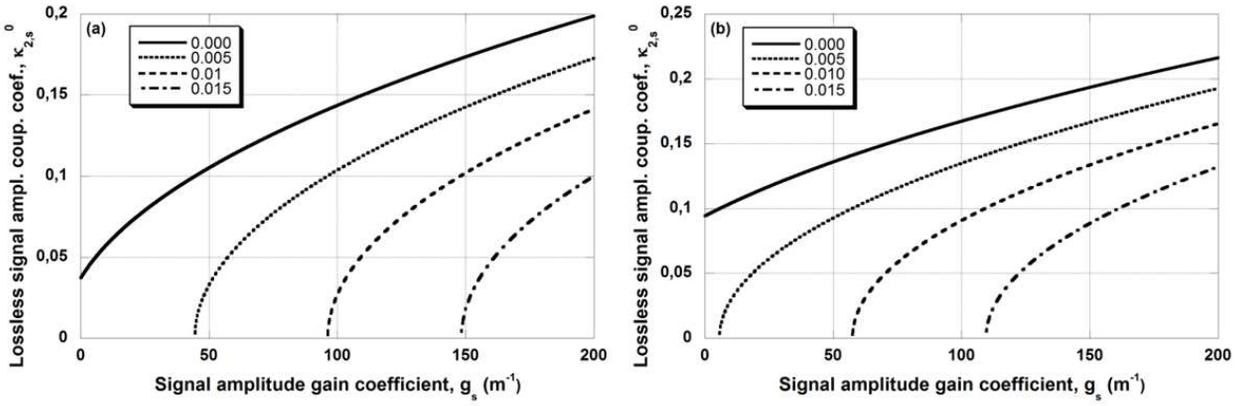

Figure 12. Lossless signal amplitude coupling coefficient $\kappa_{2,s}^0$ for CC as a function of g_s for (a) $\Gamma_{1,s}$=0.005 and (b) $\Gamma_{1,s}$=0.01, for four values of $\kappa_{1,s}^0$ [21].

In Fig. 12, the values of $\kappa_{2,s}^0$ for CC are plotted as a function of g_s for four values of $\kappa_{1,s}^0$ and for (a) $\Gamma_{1,s}$=0.005 and (b) $\Gamma_{1,s}$=0.01. Unlike the passive structure, performance output in the drop

port is not maximized for CC. The net gain that can be obtained with the parameters used in Fig. 11 is plotted in Figs. 13(a) and 13(b). Although lower net gain can be attained compared with other asymmetric configurations (see Fig. 11), significant net gain can still be achieved in case the through contribution has to be minimized.

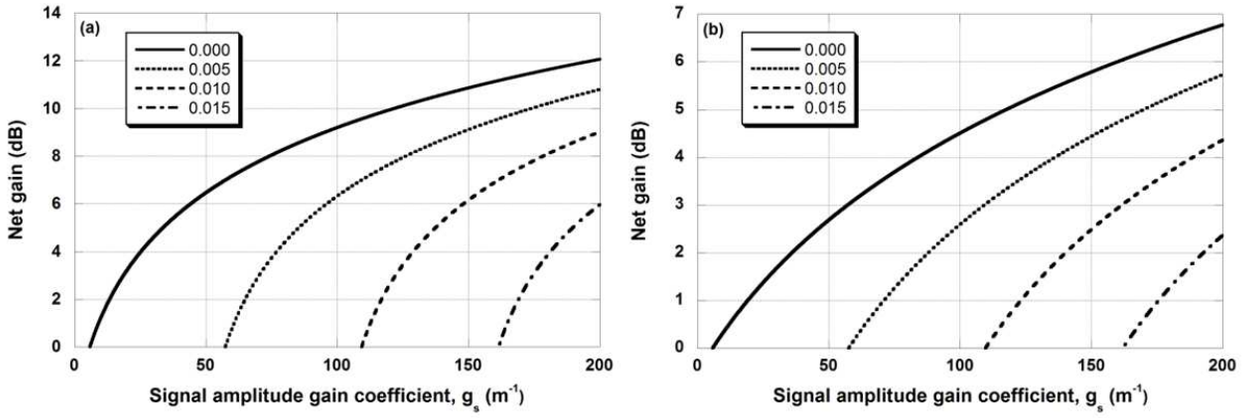

Figure 13. Net gain obtainable as a function of g_s for the asymmetric CC configurations considered in Fig.12 for (a) $\Gamma_{1,s}$=0.005 and (b) $\Gamma_{1,s}$=0.01, for four values of $\kappa_{1,s}^0$ [21].

5.3. Asymmetry influence on threshold gain

Finally, changes in g_{th} are analysed when asymmetric configurations are considered. Values of g_{th} are plotted as a function of $\Delta\kappa_{r,s}^0$ for different combinations of $(\kappa_{1,s}^0, \Gamma_{1,s})$ in Fig. 14.

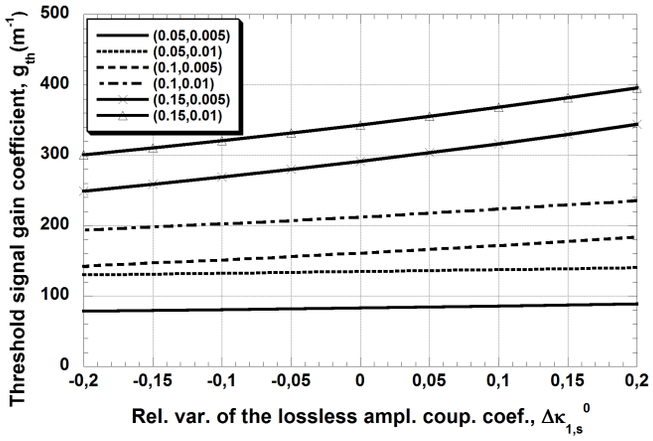

Figure 14. Variations in the threshold signal gain coefficient, g_{th}, as a function of $\Delta\kappa_{r,s}^0$ for different combinations of $(\kappa_{1,s}^0, \Gamma_{1,s})$ [21].

In Fig. 14 we can see how the necessary threshold gain value decreases for $\Delta\kappa_{r,s}^0$<0. This reduction is more significant for the higher additional coupling losses and contributes to relax the requirement for very high dopant concentrations.

http://dx.doi.org/10.5772/61767

6. Conclusions

In order to optimize RE-doped amplifying/oscillating MRRs, the coupled evolution of resonant pump and signal powers inside the integrated structure must be modelled and the interrelated passive and active characteristics must be taken into consideration. The RE ions concentration sets the attainable signal gain coefficient. This coefficient, together with the pump intensity enhancement dependences, determines the suitable combination of passive parameters (greatly influenced by the expected additional coupling losses) and RE ions doping level to achieve significant amplification or oscillation operation.

A further optimization could be achieved if non-symmetric structures are considered, allowing different values for the lossless amplitude coupling ratios and the additional coupling losses between the microring and the straight waveguides. The use of asymmetric structures can to some extent relieve the demand of a much higher signal gain coefficient and threshold gain (and accordingly dopant concentrations) as the additional losses increase. Structures with lower output coupler coupling coefficient than the input coupler one are preferable. Finally, since signal gain saturation is achieved for relatively low circulating pump powers (due to the short length of the MRR), in practice, asymmetry has little influence on pump enhancement.

Acknowledgements

This work was partially supported by the Spanish Ministry of Economy and Competitiveness under the FIS2010-20821 and TEC2013-46643-C2-2-R projects, by the Diputación General de Aragón, el Fondo Social Europeo and by a grant of the Romanian National Authority for Scientific Research, CNDIUEFISCDI, project number PN-II-PT-PCCA-2011-71 "Integrated Smart Sensor System for Monitoring of Strategic Hydrotechnical Structures HydroSens".

Author details

Juan A. Vallés[1*] and R. Gălătuş[2]

*Address all correspondence to: juanval@unizar.es

1 Department of Applied Physics and I3A, University of Zaragoza, Zaragoza, Spain

2 Optoelectronics Group, Faculty of Electronics, Telecommunications and Information Technology, Technical University of Cluj-Napoca, Cluj-Napoca, Romania

References

[1] Okamoto H, Haraguchi M and Okamoto T. Filtering characteristic of a microring resonator with a gap. Electron. Commun. Jpn. Part II-Electron. 2006;89:25–32.

[2] Little BE, Chu ST, Absil PP, Hryniewicz JV, Johnson FG, Seiferth F et al. Very high-order microring resonator filters for WDM applications. IEEE Photonics Technol. Lett. 2004;16:2263–2265.

[3] Foerst M, Niehusmann J, Plotzing T, Bolten J, Wahlbrink T, Moormann C et al. High-speed all-optical switch in ion-implanted silicon-on-insulator microring resonators. Opt. Lett. 2007;32:2046–2048.

[4] Balakrishnan M, Faccini M, Diemeer MBJ, Klein EJ, Sengo G, Driessen A et al. Microring resonator based modulator made by direct photodefinition of an electro-optic polymer. Appl. Phys. Lett. 2008;92:153310.

[5] Ramachandran A, Wang S, Clarke J, Ja S, Goad D, Wald L et al. A universal biosensing platform based on optical micro-ring resonators. Biosens. Bioelectron. 2008;23:939–944.

[6] Suter JD and Fan X. Overview of the optofluidic ring resonator: a versatile platform for label-free biological and chemical sensing. In Engineering in Medicine and Biology Society. EMBC 2009. Annual International Conference of the IEEE. 2009:1042–1044.

[7] Hunt HK and Armani AM. Label-free and chemical sensors. Nanoscale. 2010;2:1544–1559.

[8] Baaske M and Vollmer F. Optical resonator biosensors: molecular diagnostic and nanoparticle detection on an integrated platform. ChemPhysChem. 2012;13(2):427–436.

[9] Yang G, White IM and Fan X. An opto-fluidic ring resonator biosensor for the detection of organophosphorus pesticides. Sens. Actuators, B. 2009;133(1):105–112.

[10] Sun Y and Fan X. Analysis of ring resonators for chemical vapor sensor development. Opt. Express. 2008;16(14):10254–10268.

[11] Gohring JT, Dale PS and Fan X. Detection of HER2 breast cancer biomarker using the opto-fluidic ring resonator biosensor. Sens. Actuators, B.2010;146(1):226–230.

[12] Amarnath K, Grover R, Kanakaraju S and Ho PT. Electrically pumped InGaAsP-InPmicroring optical amplifiers and lasers with surface passivation. IEEE Photon. Technol. Lett. 2005;17(11):2280–2282.

[13] Hsiao HK and Winick KA. Planar glass waveguide ring resonator with gain. Opt. Express. 2007;15(26):17783–17797.

[14] He L, Ozdemir SK, Zhu J, Kim W and Zhang L. Detecting single viruses and nanoparticles using whispering gallery microlasers. Nat. nanotechnol. 2011;6(7):428–432.

[15] Bradley JD and Pollnau M. Erbium-doped integrated waveguide amplifiers and lasers. Laser. Photonics. Rev. 2011;5(3):368–403.

[16] Vallés JA. Method for accurate gain calculation of a highly Yb^{3+}/Er^{3+}-codoped waveguide amplifier in migration-assisted upconversion regime. IEEE J. Quantum. Electron. 2011;47(8):1151–1158.

[17] Li Y, Vienne G, Jiang X, Pan X, Liu X, Gu P and Tong L. Modeling rare-earth doped microfiber ring lasers. Opt. Express. 2006;14:7073–7086.

[18] Wang YH, Ma CS, Yan X and Zhang DM. Analysis for amplifying characteristics of Er^{3+}–Yb^{3+}-co-doped microring resonators. Opt. & Laser Technol. 2010;42:336–340.

[19] Vallés JA and Gălătuş R. Highly Yb^{3+}/Er^{3+}-codoped waveguide microring resonator optimized performance. IEEE Photonics Technol. Lett. 2013;25:457–459.

[20] Vallés JA and Galatus R. Modeling ofYb^{3+}/Er^{3+}-codoped microring resonators. Opt. Mater. 2015;41:126–130.

[21] Vallés JA and Gălătuş R. Requirements for gain/oscillation in Yb^{3+}/Er^{3+}-codopedmicroring resonators. Proc. SPIE. 2015;9359 Optical Components and Materials XII: 93591U.

[22] Vörckel A, Mönster M, Henschel W, Bolivar PH, Kurz H. Asymmetrically coupled silicon-on-insulator microring resonators for compact add-drop-multiplexers. IEEE Photonics. Technol. Lett. 2003;15(7),921–923.

[23] Geuzebroek DH and Driessen A. Ring-resonator-based wavelength filters. In Wavelength filters in fibre optics. Springer Berlin Heidelberg; 2006.p. 341–379.

[24] Zhao JH and Madsen CK. Optical filter design and analysis. NewYork: Wiley; 1999.

[25] Veasey DL, Funk DS, Peters PM, Sanford NA, Obarski GE, Fontaine N et al. Yb/Er-codoped and Yb-doped waveguide lasers in phosphate glass. J. Non-Cryst. Solids. 2000;263–264:369–381.

[26] Desurvire E. Erbium-doped fiber amplifiers. New York: Wiley; 1994.

[27] Taccheo S, Laporta P, Longhi S, Svelto C. Experimental analysis and theoretical modeling of a diode-pumped Er: Yb: glass microchip laser. Opt. Lett. 1995;20:889–891.

[28] Vallés JA, Ferrer A, Rebolledo MA, Ruiz de la Cruz A, Berdejo V and Solis J. Study of an optimised bidirectional pump scheme for fs-laser written Yb/Er-codoped integrated waveguides. Opt. Mater. 2010;33:231–235.

[29] Honkanen S, Ohtsuki T, Jiang S, Iraj-Najafi S, Peyghambarian N. High Er concentration phosphate glasses for planar waveguide amplifiers. Proc. SPIE. 1997;2996:32–40.

[30] Vallés JA, Rebolledo MA, Cortés J. Full characterization of packaged Er-Yb-codoped phosphate glass waveguides. IEEE J. Quantum. Electron. 2006;42:152–159.

[31] Khoptyar D, Sergeyev S and Jaskorzynska B. Homogeneous upconversion in Er-doped fibres under steady state excitation. Analytical model and its Monte-Carlo verification. J. Opt. Soc. Am. B. 2005;22(3):582–590.

[32] Gapontsev VP, Matitsin SM, Isineev AA and Kravchenko VB. Erbium glass lasers and their applications. Opt. Laser Technol. 1982;14:189–196.

[33] Majaron B, Čopič M, Lukač M and Marinček M. Influence of hole burning on laser pumping dynamics and efficiency in Yb: Er: phosphate glasses. Proc. SPIE. 1994;2138:183–190.

[34] Passaro VMN, Dell'Olio F and De Leonardis F. Sensors 2007;7:2741–2749.

[35] Ma CS, Yan X, Xu YZ, Qin ZK and Wang XY. Characteristic analysis of bending coupling between two optical waveguides.Opt. Quantum. Electron. 2005;37:1055–1067.

[36] Xia F, Sekaric L and Vlasov YA. Mode conversion losses in silicon-on-insulator photonic wire based racetrack resonators. Opt. Express. 2006;14:3872–3886.